Production of new neutron-rich isotopes near the $N = 60$ isotones ^{92}Ge and ^{93}As by in-flight fission of a 345 MeV/nucleon ^{238}U beam

Y. Shimizu,[1] T. Kubo,[1,*] T. Sumikama,[1] N. Fukuda,[1] H. Takeda,[1] H. Suzuki,[1] D. S. Ahn,[1] N. Inabe,[1] K. Kusaka,[1] M. Ohtake,[1] Y. Yanagisawa,[1] K. Yoshida,[1] Y. Ichikawa,[1] T. Isobe,[1] H. Otsu,[1] H. Sato,[1] T. Sonoda,[1] D. Murai,[2] N. Iwasa,[3] N. Imai,[4] Y. Hirayama,[5] S. C. Jeong,[5] S. Kimura,[5] H. Miyatake,[5] M. Mukai,[5] D. G. Kim,[6] E. Kim,[6] and A. Yagi[7]

[1]*RIKEN Nishina Center, RIKEN, 2-1 Hirosawa, Wako, Saitama 351-0198, Japan*
[2]*Department of Physics, Rikkyo University, Toshima, Tokyo 171-8501, Japan*
[3]*Department of Physics, Tohoku University, Aoba, Sendai, Miyagi 980-8578, Japan*
[4]*Center for Nuclear Study (CNS), The University of Tokyo, 2-1 Hirosawa, Wako, Saitama 351-0198, Japan*
[5]*Wako Nuclear Science Center (WNSC), Institute of Particle and Nuclear Studies (IPNS), High Energy Accelerator Research Organization (KEK), Wako, Saitama 351-0198, Japan*
[6]*Rare Isotope Science Project, Institute for Basic Science (IBS), Daejeon 305-811, Republic of Korea*
[7]*Department of Physics, Osaka University, Toyonaka, Osaka 560-0043, Japan*

(Received 19 December 2023; revised 8 February 2024; accepted 7 March 2024; published 8 April 2024)

A search for new neutron-rich isotopes near the $N = 60$ isotones ^{92}Ge and ^{93}As has been performed using a 345 MeV/nucleon ^{238}U beam at the RIKEN Nishina Center RI Beam Factory. Fission fragments produced were analyzed and identified in flight using the large-acceptance two-stage separator BigRIPS. We have observed a total of 15 new neutron-rich isotopes: ^{84}Cu, ^{86,87}Zn, ^{88,89}Ga, ^{91,92}Ge, ^{93,94,95}As, ^{96,97}Se, ^{99,100}Br, and ^{103}Kr.

DOI: 10.1103/PhysRevC.109.044313

I. INTRODUCTION

Since the pioneering work by Cheifetz *et al.* [1], it has been well known that the nuclear structure of neutron-rich Sr (atomic number $Z = 38$) to Mo ($Z = 42$) nuclei is characterized by the sudden onset of nuclear deformation at neutron number $N = 60$ [2–5]. Recent extensive experimental studies with rare isotope beams have revealed that such a nuclear shape transition also occurs in Rb ($Z = 37$) [6–9], Kr ($Z = 36$) [10–13], Br ($Z = 35$) [7], and Se ($Z = 34$) [14,15] nuclei at $N \approx 60$. It is intriguing to investigate whether the transition persists in nuclei with even lower Z numbers, such as As ($Z = 33$) and Ge ($Z = 32$). Furthermore, the nuclei in the relevant region are important for astrophysical nucleosynthesis through the rapid-neutron capture process [16].

The present work is aimed at expanding the frontiers of accessible nuclei in such an interesting region, in which the production of very neutron-rich isotopes with $Z \approx 32$–33 and $N \approx 60$ was investigated using in-flight fission of a ^{238}U beam. We searched for new isotopes near the $N = 60$ isotones ^{92}Ge and ^{93}As. Less neutron-rich new isotopes in the relevant Z region were observed in our previous experiments reported in Refs. [17–19].

The experiment was conducted using the BigRIPS separator [20,21] at the RIKEN Nishina Center RI Beam Factory (RIBF) [22,23]. We have observed a total of 15 new neutron-rich isotopes, ^{84}Cu, ^{86,87}Zn, ^{88,89}Ga, ^{91,92}Ge, ^{93,94,95}As, ^{96,97}Se, ^{99,100}Br, and ^{103}Kr, and deduced cross sections for the produced isotopes. This paper reports on the identification of these isotopes and the measurement of production cross sections.

II. EXPERIMENT AND ANALYSIS

The experiment was carried out using a $^{238}U^{86+}$ beam that was accelerated to 345 MeV/nucleon by the cascade operation of the RIBF accelerator complex. The uranium beam was incident on a 4-mm-thick beryllium production target [24]. Fission fragments emitted from the target were separated and identified in flight using the large-acceptance two-stage separator BigRIPS. Figure 1 shows the layout and configuration of the BigRIPS separator. The primary beam intensity was monitored by detecting light-charged particles recoiling out of the target. The uranium beam passing through the target was stopped in the beam dump located at the exit of the first dipole magnet D1 in the BigRIPS separator [25]. The beam intensity on the target was typically ≈ 11 particle nA (pnA).

The BigRIPS separator consists of two stages. The first stage from the F0 (target) to F2 foci provides isotopic separation based on a magnetic-rigidity analysis combined with an energy-loss analysis through a wedge-shaped achromatic energy degrader, while the second stage from the F3 to F7 foci provides particle identification as well as further separation using another energy degrader. The energy degraders are placed at the momentum-dispersive foci F1 and F5 located at the midpoints in these stages. The isotope separation is accomplished using slits installed at the achromatic foci F2 and F7 at their ends.

The experimental method was essentially the same as that used in our previous experiment [26], including the method of data analysis and background removal. Particle identification

*Corresponding author: kubo@ribf.riken.jp

 ©2024 American Physical Society

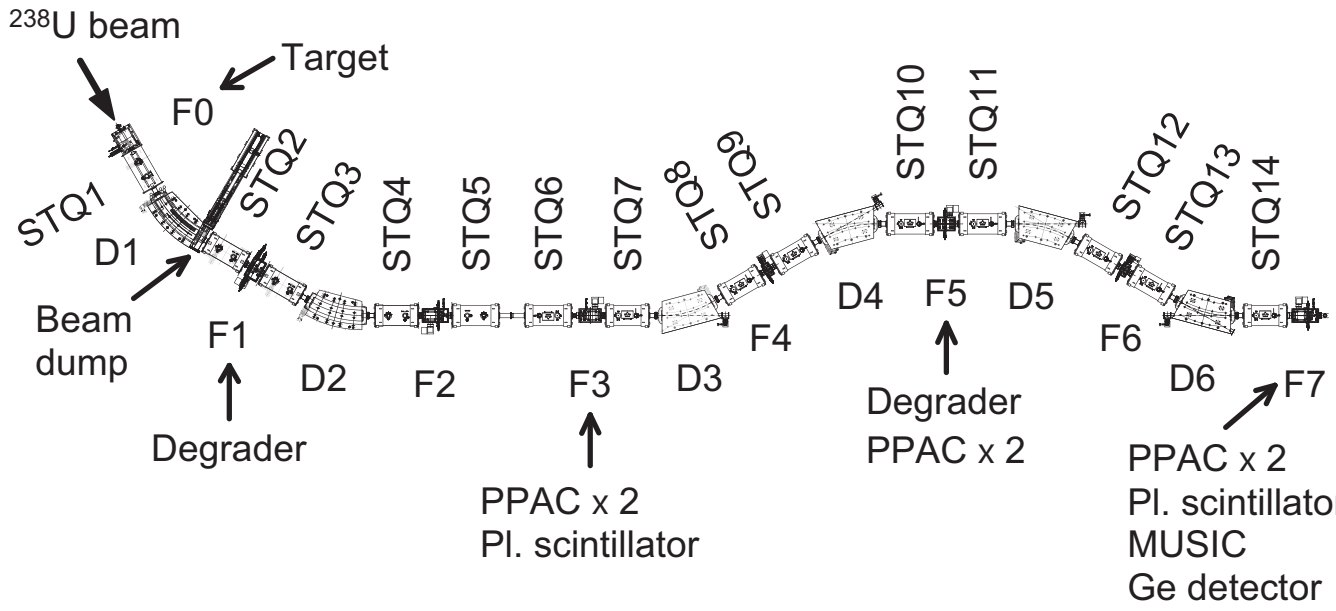

FIG. 1. Schematic layout of the BigRIPS separator. The labels STQn, Dn, and Fn indicate the positions of superconducting quadrupole triplets, room-temperature dipoles, and foci, respectively. The energy degraders and detectors are also indicated. See text for more details.

(PID) of fragments was performed in the second stage of the BigRIPS separator, using the TOF-$B\rho$-ΔE method [27], in which the mass-to-charge ratio A/Q and Z were derived for each fragment by measuring the time of flight (TOF), magnetic rigidity ($B\rho$), and energy loss (ΔE). Here, A and Q represent the mass value in atomic mass units and charge number, respectively. The TOF was measured between two thin plastic scintillators placed at the entrance (F3) and exit (F7) of the second stage, which were each 0.2 mm thick. The $B\rho$ value was determined by the trajectory reconstruction method [27] using the positions and angles measured at the F3, F5, and F7 foci with parallel plate avalanche counters (PPACs) [28]. Note that the $B\rho$ was measured at both first (F3 to F5) and second (F5 to F7) halves in the BigRIPS second stage. The ΔE was measured using a multisampling ionization chamber (MUSIC) [29] placed at the F7 focus. The fragment velocities before and after the energy degrader at the F5 focus, i.e., those in the first and second halves, were derived from the measured TOF in combination with the $B\rho$ values determined at each of these halves. The obtained velocity and $B\rho$ values were used to calculate the A/Q value of fragments. See the equations in Ref. [27] for further details. The Z value was calculated with the Bethe-Bloch formula from the measured ΔE and the derived fragment velocity. Furthermore, independent measurement of Z, referred to as Z_{F5}, was derived from the energy loss in the F5 degrader and used for removing background events. The Z_{F5} value was calculated from the $B\rho$ and velocity values before and after the F5 degrader, assuming that fragments are fully stripped. The PID was verified and calibrated by the isomer tagging method using two clover-type high-purity germanium (Ge) detectors placed at the F7 focus. Fragments were implanted into an aluminum stopper inserted and γ rays emitted from known microsecond isomers among fragments were measured. The present PID method is described in more detail in Ref. [26].

As demonstrated in Ref. [27], high-resolution PID that allows the identification of the fragment charge state Q is important in identifying new neutron-rich isotopes produced by in-flight fission of a ^{238}U beam at the present energy. High-resolution $B\rho$ and TOF measurements are required for this purpose. In the present $B\rho$ measurement with the trajectory reconstruction, we used the ion-optical transfer matrices up to the third order calculated with the COSY INFINITY code [30], implementing the detailed field maps measured as a function of magnet current [31]. For the TOF measurement, we made an empirical slewing correction to minimize the dependence of the TOF on the signal pulse height of the plastic scintillators. These allowed us to improve the $B\rho$ and TOF resolutions and hence the A/Q resolving power in PID.

Removing background events is also essential for confirming the identification of new isotopes, especially when produced with low counts. We removed inconsistent background events, such as those caused by scatterings and reactions in the detectors and degraders, signal pileups, and improper detector responses, by investigating various correlation plots created using pulse-height and timing signals from the detectors as well as beam-spot and phase-space profiles measured at the foci. Ion-optical consistency was also investigated by comparing fragment trajectories between two different foci, and inconsistent events were excluded. Furthermore, we examined the consistency between the two obtained values of atomic number, Z and Z_{F5}, by investigating the Z versus Z_{F5} plot. This allowed us to remove signal pileups in the MUSIC ΔE detector as well as reaction and charge-changing events that occurred in the F5 degrader. More details of our background removal method are described in Ref. [26].

Table I summarizes the experimental conditions. The separator settings were determined based on detailed simulations of the reaction and transmission using the LISE^{++} code [32].

TABLE I. Summary of the experimental conditions.

	S1	S2
Primary beam	$^{238}U^{86+}$ 345 MeV/nucleon	
$B\rho$[a]	8.087 Tm	
Central particle[b]	$^{94}As^{33+}$	
Production target	Be 4.00 mm	
Degrader at F1	Al 2.82 mm ($d/R = 0.115$)[c]	
Degrader at F5	Al 2.99 mm ($d/R = 0.138$)[c]	
Exit beam dump	+115.0/−125.0 mm	
F1 slit	+64.2/−64.2 mm ($\Delta P/P = \pm 3\%$)[d]	
F2 slit	+20.0/−12.0 mm	+20.0/−13.0 mm
F5 slit	+120.0/−120.0 mm	
F7 slit	+15.0/−20.0 mm	
Average beam intensity[e]	10.8 pnA	
Total dose	1.64×10^{16} particles	7.06×10^{15} particles
Average live time	66.9%	66.4%
Average trigger rate	1.22 kHz	1.31 kHz
Irradiation time	68.2 h	29.0 h

[a]Value from the magnetic field of the first dipole magnet D1.
[b]The $B\rho$ settings after the F1 focus are tuned for $^{94}As^{33+}$.
[c]d/R represents the ratio of the mean degrader thickness to the stopping range of the central particle.
[d]$\Delta P/P$ represents the corresponding momentum acceptance.
[e]1 pnA (particle nA) $= 6.24\times10^{9}$ particles/s.

The $B\rho$ settings were tuned for fully stripped $^{94}As^{33+}$ ions chosen as the central particle throughout the BigRIPS separator. In the simulations, the conditions were determined such that the overall counting rate of fragments was around 1 kHz at the F7 focus, taking into consideration the capability of our data acquisition system. After running the measurement for a while, we slightly adjusted the slit opening at the F2 focus to improve the transmission of low-Z new isotopes, such as new Cu and Zn isotopes. In Table I, the experimental conditions before and after this slit adjustment are denoted as the S1 and S2 settings, respectively. As the present $B\rho$ setting covers the region with $A/Z \approx 3$, a large number of light particles, such as triton, reached the F3 focus at the entrance of the second stage. The counting rate amounted to as much as 150 kHz. Thanks to the two-step isotope separation, few light particles could reach the F7 focus at the end of the second stage. The actual counting rate at the F7 focus was ≈ 2 kHz or less during the measurements.

III. RESULTS AND DISCUSSION

Figure 2 shows the Z versus Z_{F5} plot along with the elliptical Z gates that were used to remove background events in our data analysis. The elliptical gates are actually circles with the same 3σ radius ($= 3\times0.23$), as described in the caption of Fig. 2. The gates select the strong blobs that line up along the $Z = Z_{F5}$ line. These events are those of fully stripped fragments that did not change the Z, A, and Q values when passing through the F5 degrader. Note that if fragments are not fully stripped, such as hydrogenlike ions, the $Z = Z_{F5}$ line in the figure shifts to the right by approximately one Z unit. The tail events extending upwards from the main blobs are associated with pileups in the MUSIC ΔE detector. Those extending horizontally in the right direction originate from reactions in the F5 degrader in which one proton and two neutrons are removed from projectile fragments. Furthermore, proton-removal reactions occurring in the ΔE detector cause tail events extending downwards from the main blobs. Note that some of these tail events overlap with the neighboring main blobs in the Z versus Z_{F5} plot. It should also be noted that events from one-neutron-removal reactions and the electron stripping process in the F5 degrader, seen in our previous experiment [26], are not seen because they are located outside of the F7 slit opening in the present experiment.

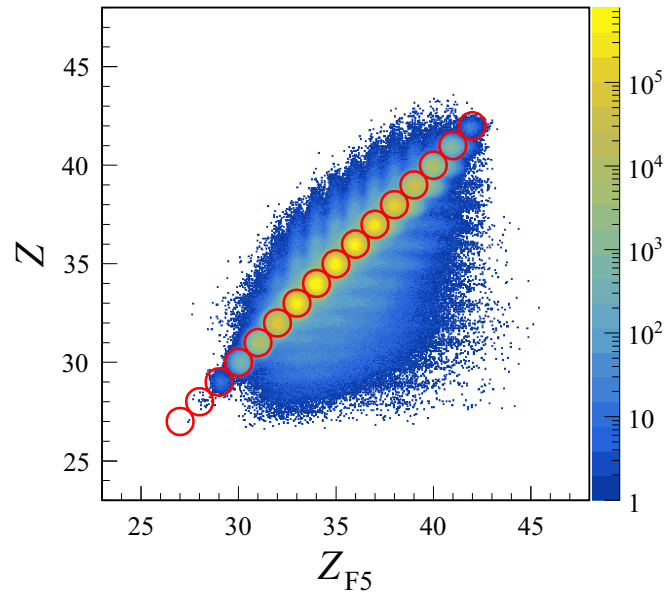

FIG. 2. Z versus Z_{F5} correlation plot for fission fragments produced in the $^{238}U + Be$ reaction at 345 MeV/nucleon. Here, Z and Z_{F5} respectively represent the atomic numbers derived from the ΔE measurement using the MUSIC detector and from the calculated energy loss in the F5 degrader. The red circles indicate the elliptical Z gates defined as $|Z - Z_0| < 3\sigma_Z$ and $|Z_{F5} - Z_0| < 3\sigma_{ZF5}$, where Z_0, σ_Z, and σ_{ZF5} represent the peak centroid, the absolute Z resolution, and the absolute Z_{F5} resolution, respectively. The resolutions are those in terms of standard deviation σ. The elliptical gates are actually circles with the same 3σ radius, because the resolutions are measured to be $\sigma_Z = \sigma_{ZF5} = 0.23$ for Z blobs strongly seen in the figure. See text for more details.

Figure 3(a) shows the Z versus A/Q PID plot obtained after all the background removals were applied including the elliptical gates shown in Fig. 2. Note that the data shown here are those summed over the two different slit conditions S1 and S2. The PID calibration was unambiguously confirmed by observing two γ rays at 81.7 and 113.8 keV from the decay of an isomeric state in ^{95}Kr at 195.5 keV with $T_{1/2} = 1.4\,\mu s$ [33] using the Ge detectors at the F7 focus. Note that fully stripped ($Q = Z$) events are dominant in the PID plot. Hydrogenlike ($Q = Z - 1$) events with A–3, located just to the left of fully stripped events with A, are hardly seen. The absolute

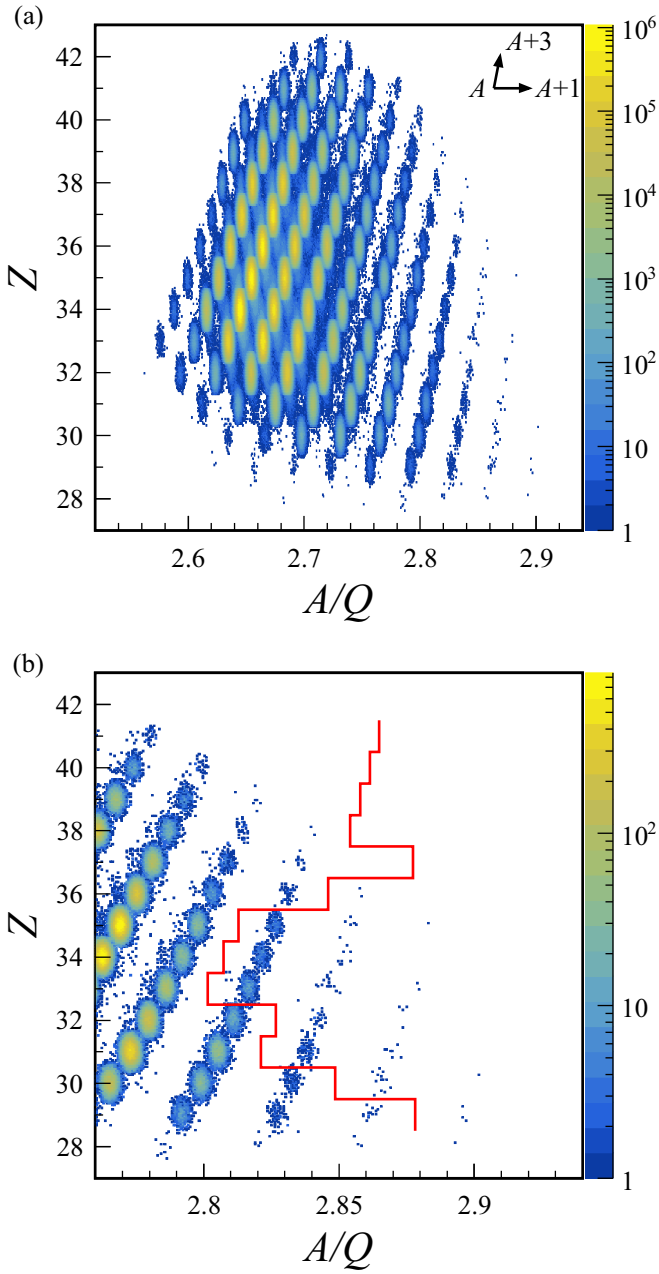

FIG. 3. Z versus A/Q particle identification plots for fission fragments produced in the ^{238}U + Be reaction at 345 MeV/nucleon. The arrows in the top panel (a) indicate that the upper-right and right-hand sides of an isotope with mass number A correspond to those with mass numbers $A+3$ and $A+1$, respectively. The bottom panel (b) shows the plot enlarged near the region of new isotopes, where the red solid lines indicate the limit of known isotopes.

A/Q resolution ($\sigma_{A/Q}$), the absolute Z resolution (σ_Z), and the absolute Z_{F5} resolution (σ_{ZF5}) were typically 1.42×10^{-3}, 0.23, and 0.23 in terms of standard deviation, respectively, which were evaluated for $^{93}As^{33+}$ events. These resolutions stay almost the same all over the isotopes seen in Fig. 3(a). Note that the elliptical gates in Fig. 2 were determined based on these σ_Z and σ_{ZF5} values. The achieved $\sigma_{A/Q}$ resolution

TABLE II. List of the new isotopes identified in this work.

Isotope	Counts[a]	Cross section (fb)	Isotope	Counts[a]	Cross section (fb)
^{84}Cu	3	[b]	^{94}As	12	8.7×10^{1}
^{86}Zn	11	1.7×10^{2}	^{95}As	2	1×10^{1}
^{87}Zn	1	7	^{96}Se	230	1.98×10^{3}
^{88}Ga	75	6.6×10^{2}	^{97}Se	6	5×10^{1}
^{89}Ga	6	4×10^{1}	^{99}Br	194	1.63×10^{3}
^{91}Ge	26	2.0×10^{2}	^{100}Br	5	4×10^{1}
^{92}Ge	4	3×10^{1}	^{103}Kr	2	2×10^{1}
^{93}As	543	4.57×10^{3}			

[a]The counts were obtained by integrating over the rectangular area defined as $|Z-Z_0|<2\sigma_Z$ and $|A/Q-(A/Q)_0|<2\sigma_{A/Q}$ in the Z versus A/Q PID plot, where Z_0 and $(A/Q)_0$ represent the peak centroids of Z and A/Q, respectively, and σ_Z and $\sigma_{A/Q}$ are the absolute Z and A/Q resolutions in terms of standard deviation, respectively.
[b]The cross section is not shown for ^{84}Cu because its mean position at the F2 focus is located outside the slit opening.

can clearly resolve the closely neighboring fully stripped and hydrogenlike peaks, although the latter is not actually seen. Figure 3(b) shows an enlarged PID plot near the region of new isotopes. The red solid lines in the figure indicate the limit of known isotopes [17–19,34]. The figure exhibits sufficient separation among the blobs of various nuclides as well as excellent background rejection in the region of new isotopes.

Pileups and reactions occurring in the ΔE detector and the F5 degrader created some tail events in the Z determination as mentioned above. Even though tight gates are applied to the main blobs in the Z versus Z_{F5} plot, these tail events leak into the next neighboring gates with $Z\pm1$, as seen in Fig. 2. As a result, a small number of tail events in the Z determination are left unremoved, as seen in Fig. 3(a). The ratios of such tail events to their parent events are estimated to be as small as 2.3×10^{-4}, 2.2×10^{-4}, and 1.3×10^{-6} for the pileups in the ΔE detector, the proton-removal reactions in the ΔE detector, and the one-proton- and two-neutron-removal reactions in the F5 degrader, respectively. Furthermore, the ratio of hydrogenlike to fully stripped events is also estimated to be as small as 3.4×10^{-6}. Because these ratios are so small, the observed background contamination in the region of new isotopes is quite low, as seen in Fig. 3(b). Note that these ratios were obtained with strongly populated isotopes in the known region.

The proton-removal reactions in the ΔE detector not only create the Z tails extending downwards but also slightly affect the A/Q determination for the tails, as seen in Fig. 3(a). This is because the ΔE detector is placed between the PPAC detectors that measure the fragment trajectories at the F7 focus. The trajectory changes caused by the reactions affect the trajectory reconstruction and hence the A/Q determination. The effects are largest when the reactions occur in the entrance region of the ΔE detector including the relatively thick window foil [29]. In this case, the Z tails are also maximized.

Figure 4 shows the projected one-dimensional A/Q spectra for the Cu, Zn, Ga, Ge, As, Se, Br, and Kr isotopes, which were obtained by gating the two-dimensional PID plot with Z gates set to $Z\pm0.46$ ($2\sigma_Z$). The peaks labeled with mass num-

bers correspond to the new isotopes identified in this work. The solid lines in the A/Q spectra indicate the locations of new isotope peaks expected from the AME2020 atomic mass evaluation [35], while the dotted lines show their $\pm 2\sigma_{A/Q}$ width. As seen in the figure, the observed A/Q values of new isotopes are consistent with the AME2020 atomic mass evaluation, supporting our identification of the new isotopes. In total, we have produced and identified the following 15 new neutron-rich isotopes: ^{84}Cu, ^{86,87}Zn, ^{88,89}Ga, ^{91,92}Ge, ^{93,94,95}As, ^{96,97}Se, ^{99,100}Br, and ^{103}Kr. The frontiers of known isotopes have been significantly expanded in the neutron-rich side. The new isotopes identified are listed in Table II along with their observed counts and deduced production cross sections.

Figure 5 shows the measured production cross sections for the observed isotopes as a function of mass number along with the theoretical predictions. The measured cross sections were derived using the separator transmission efficiency simulated with the LISE^{++} code in the Monte Carlo mode. Note that cross sections are not shown for isotopes whose mean positions were located outside the slit opening at the F2 focus, because the transmission efficiency may not be properly simulated. Note also that those measured in our previous experiments [17,19] are included in Fig. 5. We estimate that the present cross-section measurements have a systematic error of $\approx 40\%$, mainly resulting from the determination of the beam intensity and the evaluation of the transmission efficiency. Although some odd-even staggering is seen, the measured cross sections shown in Fig. 5 on a logarithmic scale smoothly decrease with increasing mass number, exhibiting an expected behavior. Furthermore, the cross sections measured in our present and previous experiments agree well. These results support the validity and consistency of our present measurement including the identification of new isotopes.

The solid and dashed lines in Fig. 5 show predictions from two different abrasion fission (AF) model calculations with the LISE^{++} code, the three excitation-energy region (3EER) model [36], and the initial fissile nuclei (IFN) analyzer model [37]. In the 3EER model, the fissile nuclei created in the abrasion stage of in-flight fission are represented by three different nuclei with low, medium, and high excitation energies, while the IFN analyzer model makes calculations for all the fissile nuclei that have significant contributions to producing fission fragments. The latter has recently been implemented in the LISE^{++} code to allow more realistic AF calculations. We used LISE^{++} version 8.4.1 and the standard parameters described in Refs. [17,38] for the 3EER model to be consistent with our previous publications. The recommended parameters (version 12.1.2) given in Ref. [37] were used for the IFN analyzer model. The measured cross sections are fairly well reproduced by the 3EER model, while the IFN analyzer model exhibits somewhat increasing discrepancies with increasing N (decreasing cross sections), especially in the region of the observed new isotopes. The creation process of fissile nuclei in the abrasion stage and/or the succeeding fission process might still remain to be improved in the model. Further accumulation of cross-section data would be needed for a wide Z range of fission fragments with large N numbers.

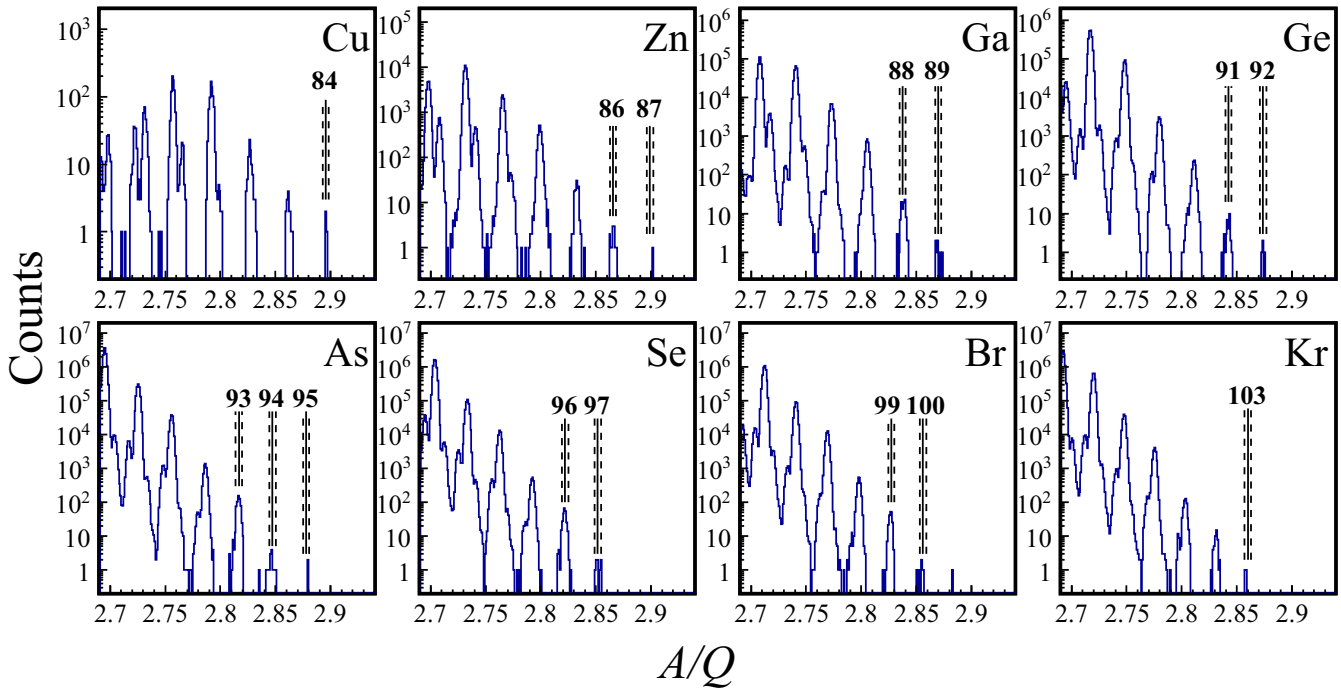

FIG. 4. A/Q spectra of the Cu, Zn, Ga, Ge, As, Se, Br, and Kr isotopes. The peaks labeled with mass numbers correspond to the new isotopes identified in this work. The solid and dotted lines indicate the expected location of the new isotope and the $\pm 2\sigma_{A/Q}$ range, respectively, where $\sigma_{A/Q}$ represents the absolute A/Q resolution in terms of standard deviation. Note that ^{101}Br was already observed in our previous work [19]. See text for more details.

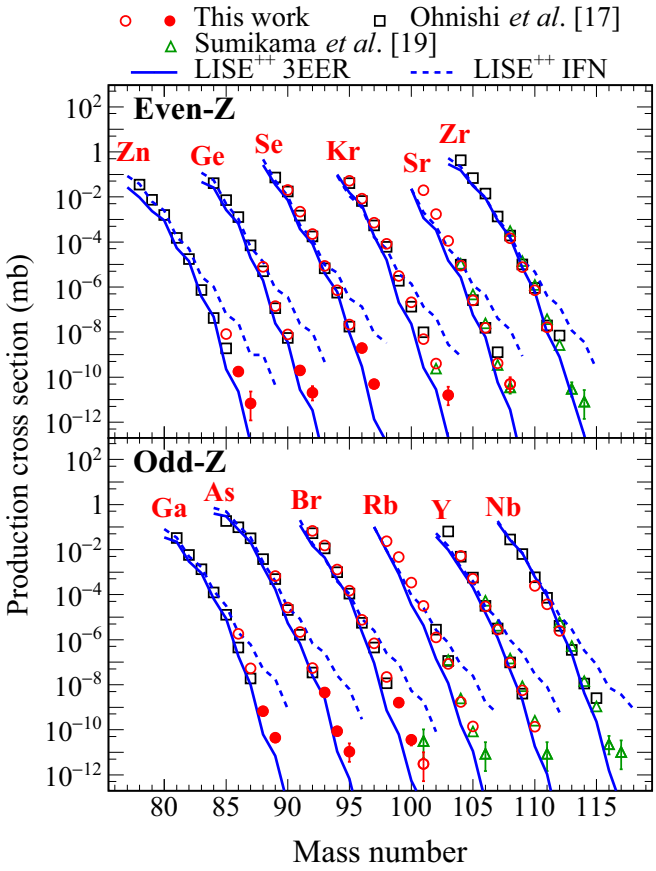

FIG. 5. Measured production cross sections of neutron-rich isotopes from the ^{238}U + Be reaction at 345 MeV/nucleon shown as a function of mass number along with theoretical predictions. The errors shown are statistical only. The open and filled circles indicate those measured in this work for known and new isotopes, respectively. The solid and dashed lines show those predicted from the LISE^{++} abrasion fission (AF) calculations, using the three excitation-energy region (3EER) model and the initial fissile nuclei (IFN) analyzer model, respectively. The squares and triangles represent those from our previous measurements in Ref. [17] and Ref. [19], respectively. See text for more details.

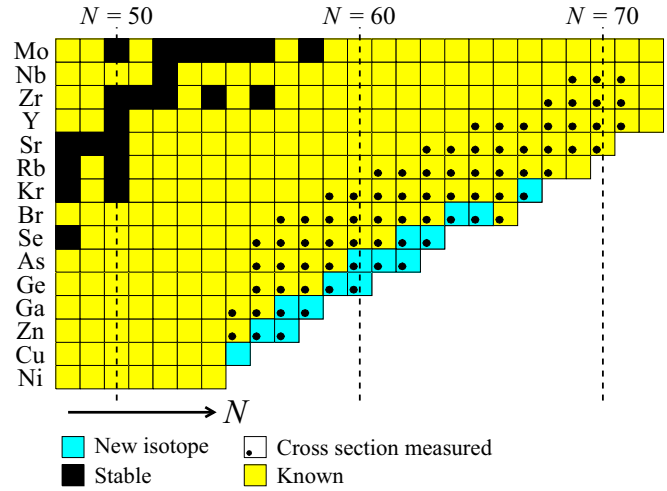

FIG. 6. Section of nuclear chart showing the new isotopes observed in this work. The black squares indicate stable isotopes. The known and new isotopes are labeled in yellow and light blue, respectively. The squares with a small dot indicate isotopes whose production cross sections were measured in this work. Note that ^{101}Br has been previously observed [19].

IV. SUMMARY

In summary, we have conducted a search for new isotopes using the in-flight fission of a 345-MeV/nucleon ^{238}U beam at the RIKEN RIBF. The production, separation, and identification of fission fragments were carried out with the BigRIPS separator. A total of 15 new isotopes in the very neutron-rich region near $Z = 32 - 33$ and $N = 60$ were observed. The production cross sections were also measured for produced isotopes and compared with the theoretical calculations.

The nuclear chart in Fig. 6 shows the new isotopes observed in this work and the isotopes whose production cross sections were measured. The frontiers of known isotopes have been significantly expanded, including As and Ge isotopes. For As isotopes, three new isotopes ^{93,94,95}As were observed, reaching as far as ^{95}As, which has two more neutrons than ^{93}As at $N = 60$. For Ge isotopes, two new isotopes ^{91,92}Ge were observed, reaching ^{92}Ge at $N = 60$. Experimental studies on the properties and nuclear structure of these $N = 60$ nuclei and their neighboring nuclei will be an important challenge for new-generation rare isotope beam facilities [23], where orders of magnitude higher beam intensities become available in future.

ACKNOWLEDGMENTS

The experiment was carried out under Program No. DA14-02 at the RIBF operated by the RIKEN Nishina Center and the Center for Nuclear Study, The University of Tokyo. The authors are grateful to the RIBF accelerator crew for providing the ^{238}U primary beam. T.K. is grateful to Y. Yano and H. Sakurai for their encouragement during the writing of this paper. He also wishes to thank D. Suzuki and P. Doornenbal for their useful advice.

[1] E. Cheifetz, R. C. Jared, S. G. Thompson, and J. B. Wilhelmy, Experimental information concerning deformation of neutron rich nuclei in the $A\sim100$ region, Phys. Rev. Lett. **25**, 38 (1970).

[2] H. Wollnik, F. K. Wohn, K. D. Wünsch, and G. Jung, Experimental indication of the onset of nuclear deformation in neutron-rich Sr isotopes at mass 98, Nucl. Phys. A **291**, 355 (1977).

[3] U. Hager, A. Jokinen, V.-V. Elomaa, T. Eronen, J. Hakala, A. Kankainen, S. Rahaman, J. Rissanen, I. D. Moore, S. Rinta-Antila, A. Saastamoinen, T. Sonoda, and J. Äystö, Precision

mass measurements of neutron-rich yttrium and niobium isotopes, Nucl. Phys. A. **793**, 20 (2007), and references therein.
[4] K. Heyde and J. L. Wood, Shape coexistence in atomic nuclei, Rev. Mod. Phys. **83**, 1467 (2011), and references therein.
[5] E. Clément *et al.*, Spectroscopic quadrupole moments in ^{96,98}Sr: Evidence for shape coexistence in neutron-rich strontium isotopes at $N = 60$, Phys. Rev. Lett. **116**, 022701 (2016).
[6] C. Thibault, F. Touchard, S. Büttgenbach, R. Klapisch, M. de Saint Simon, H. T. Duong, P. Jacquinot, P. Juncar, S. Liberman, P. Pillet, J. Pinard, J. L. Vialle, A. Pesnelle, and G. Huber, Hyperfine structure and isotope shift of the D_2 line of $^{76-98}$Rb and some of their isomers, Phys. Rev. C **23**, 2720 (1981).
[7] D. Kameda *et al.*, Observation of new microsecond isomers among fission products from in-flight fission of 345 MeV/nucleon ^{238}U, Phys. Rev. C **86**, 054319 (2012).
[8] M. Rudigier, G. S. Simpson, J. M. Daugas, A. Blazhev, C. Fransen, G. Gey, M. Hackstein, J. Jolie, U. Köster, T. Malkiewicz, T. Materna, M. Pfeiffer, M. Ramdhane, J.-M. Régis, W. Rother, T. Thomas, N. Warr, D. Wilmsen, J. Le Bloas, and N. Pillet, Delayed γ-ray and conversion-electron spectroscopy of $A = 97$ fission fragments, Phys. Rev. C **87**, 064317 (2013).
[9] C. Sotty *et al.*, $^{97}_{37}$Rb$_{60}$: The cornerstone of the region of deformation around A∼100, Phys. Rev. Lett. **115**, 172501 (2015).
[10] S. Naimi, G. Audi, D. Beck, K. Blaum, Ch. Böhm, Ch. Borgmann, M. Breitenfeldt, S. George, F. Herfurth, A. Herlert, M. Kowalska, S. Kreim, D. Lunney, D. Neidherr, M. Rosenbusch, S. Schwarz, L. Schweikhard, and K. Zuber, Critical-point boundary for the nuclear quantum phase transition near $A = 100$ from mass measurements of ^{96,97}Kr, Phys. Rev. Lett. **105**, 032502 (2010).
[11] M. Albers *et al.*, Evidence for a smooth onset of deformation in the neutron-rich Kr isotopes, Phys. Rev. Lett. **108**, 062701 (2012).
[12] J. Dudouet *et al.*, $^{96}_{36}$Kr$_{60}$ – Low-Z boundary of the island of deformation at $N = 60$, Phys. Rev. Lett. **118**, 162501 (2017).
[13] F. Flavigny *et al.*, Shape evolution in neutron-rich krypton isotopes beyond $N = 60$: First spectroscopy of ^{98,100}Kr, Phys. Rev. Lett. **118**, 242501 (2017).
[14] S. Chen *et al.*, Low-lying structure and shape evolution in neutron-rich Se isotopes, Phys. Rev. C **95**, 041302(R) (2017).
[15] C. Lizarazo *et al.*, Metastable states of ^{92,94}Se: Identification of an oblate K isomer of ^{94}Se and the ground-state shape transition between $N = 58$ and 60, Phys. Rev. Lett. **124**, 222501 (2020).
[16] J. J. Cowan, C. Sneden, J. E. Lawler, A. Aprahamian, M. Wiescher, K. Langanke, G. Martínez-Pinedo, and F. Thielemann, Origin of the heaviest elements: The rapid neutron-capture process, Rev. Mod. Phys. **93**, 015002 (2021).
[17] T. Ohnishi *et al.*, Identification of 45 new neutron-rich isotopes produced by in-flight fission of a ^{238}U beam at 345 MeV/nucleon, J. Phys. Soc. Jpn. **79**, 073201 (2010).
[18] T. Sumikama *et al.*, Observation of new neutron-rich Mn, Fe, Co, Ni, and Cu isotopes in the vicinity of ^{78}Ni, Phys. Rev. C **95**, 051601(R) (2017).
[19] T. Sumikama *et al.*, Observation of new neutron-rich isotopes in the vicinity of ^{110}Zr, Phys. Rev. C **103**, 014614 (2021).
[20] T. Kubo, In-flight RI beam separator BigRIPS at RIKEN and elsewhere in Japan, Nucl. Instrum. Methods Phys. Res. Sect. B **204**, 97 (2003).
[21] T. Kubo, D. Kameda, H. Suzuki, N. Fukuda, H. Takeda, Y. Yanagisawa, M. Ohtake, K. Kusaka, K. Yoshida, N. Inabe, T. Ohnishi, A. Yoshida, K. Tanaka, and Y. Mizoi, BigRIPS separator and ZeroDegree spectrometer at RIKEN RI Beam Factory, Prog. Theor. Exp. Phys. **2012**, 03C003 (2012).
[22] Y. Yano, The RIKEN RI beam factory project: A status report, Nucl. Instrum. Methods Phys. Res. Sect. B **261**, 1009 (2007).
[23] T. Kubo, Recent progress of in-flight separators and rare isotope beam production, Nucl. Instrum. Methods Phys. Res. Sect. B **376**, 102 (2016).
[24] A. Yoshida, Y. Yanagisawa, and T. Kubo, Beam-spot temperature monitoring on the production target at the BigRIPS separator, Nucl. Instrum. Methods Phys. Res. Sect. A **655**, 10 (2011).
[25] K. Yoshida, N. Fukuda, Y. Yanagisawa, N. Inabe, Y. Mizoi, and T. Kubo, High-power beam dump system for the BigRIPS fragment separator at RIKEN RI Beam Factory, Nucl. Instrum. Methods Phys. Res. Sect. B **317**, 373 (2013).
[26] Y. Shimizu *et al.*, Observation of new neutron-rich isotopes among fission fragments from in-flight fission of 345 MeV/nucleon ^{238}U: Search for new isotopes conducted concurrently with decay measurement campaigns, J. Phys. Soc. Jpn. **87**, 014203 (2018).
[27] N. Fukuda, T. Kubo, T. Ohnishi, N. Inabe, H. Takeda, D. Kameda, and H. Suzuki, Identification and separation of radioactive isotope beams by the BigRIPS separator at the RIKEN RI Beam Factory, Nucl. Instrum. Methods Phys. Res. Sect. B **317**, 323 (2013).
[28] H. Kumagai, T. Ohnishi, N. Fukuda, H. Takeda, D. Kameda, N. Inabe, K. Yoshida, and T. Kubo, Development of parallel plate avalanche counter (PPAC) for BigRIPS fragment separator, Nucl. Instrum. Methods Phys. Res. Sect. B **317**, 717 (2013).
[29] Y. Sato, A. Taketani, N. Fukuda, H. Takeda, D. Kameda, H. Suzuki, Y. Shimizu, D. Nishimura, M. Fukuda, N. Inabe, H. Murakami, K. Yoshida, and T. Kubo, Energy resolution of gas ionization chamber for high-energy heavy ions, Jpn. J. Appl. Phys. **53**, 016401 (2014).
[30] K. Makino and M. Berz, COSY INFINITY Version 9, Nucl. Instrum. Methods Phys. Res. Sect. A **558**, 346 (2006).
[31] H. Takeda, T. Kubo, K. Kusaka, H. Suzuki, N. Inabe, and J. A. Nolen, Extraction of 3D field maps of magnetic multipoles from 2D surface measurements with applications to the optics calculations of the large-acceptance superconducting fragment separator BigRIPS, Nucl. Instrum. Methods Phys. Res. Sect. B **317**, 798 (2013).
[32] O. B. Tarasov and D. Bazin, LISE^{++}: Radioactive beam production with in-flight separators, Nucl. Instrum. Methods Phys. Res. Sect. B **266**, 4657 (2008), and references therein; LISE^{++} manual, Michigan State University, http://groups.nscl.msu.edu/lise/lise.html.
[33] J. Genevey, R. Guglielmini, R. Orlandi, J. A. Pinston, A. Scherillo, G. Simpson, I. Tsekhanovich, N. Warr, and J. Jolie, First observation of low-lying excited states in the very neutron-rich ^{95}Kr, Phys. Rev. C **73**, 037308 (2006).
[34] M. Bernas, C. Engelmann, P. Armbruster, S. Czajkowski, F. Ameil, C. Böckstiegel, Ph. Dessagne, C. Donzaud, H. Geissel, A. Heinz, Z. Janas, C. Kozhuharov, Ch. Miehé, G. Münzenberg, M. Pfützner, W. Schwab, C. Stéphan, K. Sümmerer, L. Tassan-Got, and B. Vass, Discovery and cross-section measurement

of 58 new fission products in projectile-fission of 750·A MeV ^{238}U, Phys. Lett. B **415**, 111 (1997).

[35] W. J. Huang, M. Wang, F. G. Kondev, G. Audi, and S. Naimi, The AME 2020 atomic mass evaluation (I). Evaluation of input data, and adjustment procedures, Chin. Phys. C **45**, 030002 (2021); M. Wang, W. J. Huang, F. G. Kondev, G. Audi, and S. Naimi, The AME 2020 atomic mass evaluation (II). Tables, graphs and references, *ibid.* **45**, 030003 (2021).

[36] O. B. Tarasov, LISE^{++} manual, Michigan State University, https://lise.nscl.msu.edu/10_1/10_1_127_highZ_AF.pdf.

[37] O. B. Tarasov, LISE^{++} manual, Michigan State University, http://lise.nscl.msu.edu/10_1/11_0_28_IFN_search.pdf.

[38] H. Suzuki *et al.*, Production cross section measurements of radioactive isotopes by BigRIPS separator at RIKEN RI Beam Factory, Nucl. Instrum. Methods Phys. Res. Sect. B **317**, 756 (2013).